A Theoretical Study of the Accuracy of Tomographic Retrieval of Cloud Liquid with an Airborne Radiometer

J. F. DRAKE AND J. WARNER

National Center for Atmospheric Research, Boulder, Colorado*

(Manuscript received 5 March 1987, in final form 2 November 1987)

ABSTRACT

Prior studies of the technique of inferring the liquid water distribution in a cloud with microwave cloud tomography have concentrated on the use of ground-based instruments. An extension of the technique to the analysis of measurements at 31.65 GHz that can be made with an airborne radiometer is described. An improved retrieval method is presented and applied to simulated measurements to determine the accuracy attainable under various conditions. The results of the simulation study are summarized in a figure relating the average error in a retrieval to the size of the cloud, the maximum liquid water content, the resolution, and the number of measurements to be made with a sensitive radiometer. The error is of the order of 10% of the maximum liquid water content for nonprecipitating clouds with a maximum water content greater than 1 g m^{-3} for a spatial resolution of a few hundred meters. The question of the uniqueness of a retrieval and the likely spatial distribution of error are studied by analyzing the linearized radiative transfer equation. Absorption and scattering coefficients for a range of liquid precipitation rates are computed with Mie theory. The results support a previous judgment that roughly 1 mm h^{-1} is the largest precipitation rate allowing the technique to remain useful.

1. Introduction

A remote sensing technique that permits the liquid water distribution in a complete vertical cross section of a cloud to be inferred from data taken in two or three minutes was presented by Warner et al. (1985, hereafter referred to as WDK) who assessed its accuracy with computer simulation. As long as the cloud does not contain large drops the technique does not depend on knowing the distribution of droplet sizes. It requires that the atmospheric radiance at a frequency of 31.65 GHz (0.95 cm wavelength) be measured in many directions by two precision, narrow beam, microwave radiometers at fixed sites. The thermodynamic structure of the clear atmosphere in the cloud's vicinity, which is assumed to be known approximately, implies a certain angular variation of radiance in the absence of cloud. The distribution of cloud liquid is determined by analyzing the measurements of radiation emitted by the cloud and the surrounding atmosphere with a method of computed tomography. Warner et al. (1986) used this technique to estimate the liquid distribution in Colorado cumuli.

Another possible configuration discussed briefly by WDK is shown schematically in Fig. 1. An aircraft carries a single radiometer along a horizontal line passing just under a cloud. The instrument switches automatically between two fixed antennas which are elevated equal angles above the longitudinal axis of the aircraft; one points forward, the other aft. The movement of the aircraft relative to the cloud generates a set of measurements from different locations with each antenna. This scanning in location replaces the angular scanning of the ground-based instruments.

The airborne configuration is preferable for several reasons. The planetary boundary layer is geometrically thin but, at least in the microwave region, optically thick relative to the rest of the clear atmosphere. Turbulent fluctuations in temperature and humidity, which induce corresponding changes in optical properties, are also likely to be greater in the boundary layer than above it. The resulting uncertainty in the optical characteristics of the boundary layer, while not large, implies that a retrieval from measurements taken at the surface is likely to be less accurate than one from measurements taken aloft. The smaller number of radiometers and supporting devices and the greater flexibility of a mobile platform also make it easier to choose the location of cloud studies.

Since the geometry of measurement by an airborne radiometer differs appreciably from the configuration previously studied, a separate assessment of the accuracy attainable with the new configuration is needed. The present paper describes an improved retrieval algorithm and its use in analyzing a series of simulations of airborne radiometer measurements to determine

* The National Center for Atmospheric Research is sponsored by the National Science Foundation.

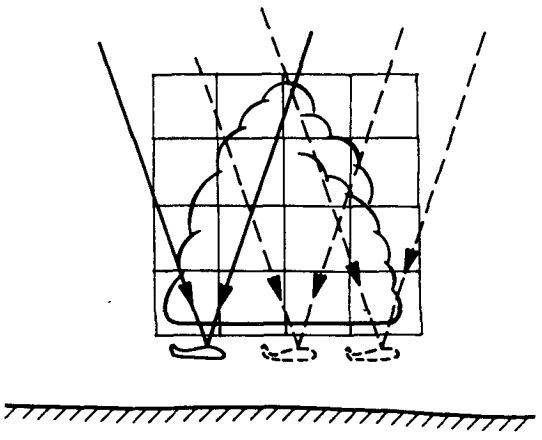

FIG. 1. Equipment configuration with an airborne radiometer. The retrieval domain is divided into square elements as discussed in the text.

how the accuracy of retrieved fields of cloud liquid depends on the properties of clouds, the climates in which they form, and the observational and analytic choices that might be made. The local properties of the radiative transfer operator governing the inverse problem are analyzed to study the distribution of errors in a retrieval and to describe the character of the spatial modes of the field of cloud liquid that can be retrieved. Finally, the limits of the technique with clouds containing large drops are examined by applying Mie theory.

2. A description of the simulation and retrieval procedures

a. The calculation of simulated measurements

The downward flux of natural, thermal, microwave radiation originates in sources beyond the atmosphere as well as within it, and the measure of its strength is its radiance. Nonprecipitating clouds, the principal concern of this study, scatter a negligible amount of radiation at the frequency considered; other scatterers are also not important (see section 5). This implies that the flux is attenuated only by absorption and that its sources can only be emitters at altitudes higher than where the radiation is observed.

The radiance at a radiometer antenna, I, may be separated into three parts. The first is emitted by the clear atmosphere between the antenna and the cloud and is denoted by I_l. The effect of absorption will be represented by introducing τ, the transmission factor between two points along the line of propagation of the radiation. This factor is the fraction of the incoming radiance that remains after passage between the points. The transmission through the clear atmosphere below the cloud is denoted by τ_l. The second part is emitted by the cloud and attenuated in the clear air below it and may be expressed as $\tau_l I_c$, where I_c is the radiance as the flux emerges from the cloud, and τ_c is defined as the transmission through the cloud along the line of propagation. The third part, emitted by the upper atmosphere and extraterrestrial sources, is attenuated by the cloud and lower atmosphere and may be expressed as $\tau_l \tau_c I_u$, where I_u is the radiance as the downward flux enters the upper cloud surface. Combining the parts gives

$$I = I_l + \tau_l(I_c + \tau_c I_u) \tag{1}$$

for the radiance at the antenna.

The variation of radiance along the line of propagation is governed by the radiative transfer equation for a medium in local thermodynamic equilibrium that does not scatter; as discussed in WDK, the emission coefficient is then equal to the absorption coefficient and the source function is simply the Planck function. The solution of this form of the radiative transfer equation may be written explicitly and used to express I_c, I_l and I_u. First, note that $\tau(l_1, l_2)$, the transmission between two points at distances l_1 and l_2 along the line of propagation ($l_1 \leq l_2$), takes the form

$$\tau(l_1, l_2) = \exp\left(-\int_{l_1}^{l_2} \alpha ds\right), \tag{2}$$

where α is the absorption coefficient per unit length and s is the distance along the line of propagation. Then I_c is given by

$$I_c = \int_{s_1}^{s_2} \alpha\tau(s_1, s)B ds \tag{3}$$

where B is the Planck function and s_1 and s_2 are the distances to the points where the line of propagation extending from the antenna enters and leaves the cloud. Note that $\tau_c = \tau(s_1, s_2)$. Since the frequency is fixed, B depends only on the temperature at the distance s. Equation (3) may be interpreted as saying that the medium between s and $s + ds$ contributes to the flux reaching the cloud boundary by the strength of the source, $B\alpha ds$, diminished by the transmission between s and the boundary, $\tau(s_1, s)$.

As (2) and (3) make evident, I_c and τ_c depend on the *distribution* of α along the part of the line of propagation that intersects the cloud. The I_l, I_u and τ_l values depend on the distribution of α along the line in the respective clear regions through expressions so similar to those above that they will be omitted. It may be seen from (1), then, that I depends on the distribution, along the entire line of propagation leading to the antenna, of α and temperature (through the temperature dependence of B). The relation between I and α is nonlinear.

We have emphasized the physical properties of the atmosphere associated with the emission and absorption of the radiative flux propagating along a single line, but each measurement depends on the flux from a manifold of such lines which reach a radiometer antenna from different directions as it is carried by the

aircraft. It is necessary, then, to speak of the direction of a line of propagation, θ, and the location of an antenna at a certain time, $\mathbf{r}(t)$, because $I = I(r, \theta)$. Temporal changes in the radiative properties of the cloud and surrounding atmosphere during the two or three minutes it takes to gather the data for a retrieval are assumed to be negligible; otherwise the radiance I would also depend explicitly on time.

A radiometer measurement, $\bar{I}$, is the average over the measurement time t_M, during which the aircraft travels a short distance, of the convolution of I with the antenna pattern, G_w. Variations in the aircraft roll angle and the width of the antenna pattern lateral to the plane of the retrieval are assumed to be small enough that only lines of propagation in the plane need to be considered. The direction of each such line is specified by the angle it makes with the horizontal, and θ will be taken to be this angle. The type of antenna most suited to this application has negligible side lobes and an antenna pattern that decreases exponentially with the square of the angular departure from the central axis ξ:

$$G_w(\xi) = \frac{1}{w}\left(\frac{\beta}{\pi}\right)^{1/2} \exp\left[-\beta\left(\frac{\xi}{w}\right)^2\right], \tag{4}$$

where β is a dimensionless constant and w is the angular separation of half-power points, i.e., the beamwidth [cf. (4) in WDK]. $\bar{I}$ is given by

$$\bar{I} = \frac{1}{t_M}\int_t^{t+t_M}\int_{\theta_a-\pi/2}^{\theta_a+\pi/2} IG_w(\theta - \theta_a)d\theta dt', \tag{5}$$

where θ_a is the angle of the antenna axis.

The angle θ_a will vary slightly during an aircraft traverse beneath real clouds because of small changes in aircraft attitude. Since we assume that the attitude would be recorded along with the other quantities to be observed, at least in principle this variability does not add uncertainty to the retrieval process. The same consideration applies to aircraft speed. It therefore seemed permissible, when generating synthetic measurements to perform the simulations described below, to fix the aircraft pitch angle at a typical value, which made θ_a for each antenna constant.

Measurements are simulated for an atmosphere with specified thermodynamic properties which contains a cloud. The number of measurements is denoted by m. The value of $\bar{I}$ that the radiometer would measure in each successive interval during a traverse is computed from (5). Wherever α is needed it is calculated from the gaseous absorption coefficient α_g, the liquid density ρ_l, and the absorption coefficient per unit mass density of liquid water κ. These quantities depend on the thermodynamic properties of the atmosphere. The formulas used for α_g and κ appear in the appendix of WDK. Normally distributed random numbers are added to the computed values of $\bar{I}$ to represent the effect of measurement uncertainty. The normal distribution has zero mean and a standard deviation appropriate to t_M and the accuracy of the radiometer simulated. Each measurement is regarded as a component of the vector $\tilde{\mathbf{I}}$ (the tilde indicates the difference between a partially random component of $\tilde{\mathbf{I}}$ and a deterministic $\bar{I}$).

The value of $\bar{I}$ for a measurement is given in (5) as a double integral of an integrand containing I, which itself depends on integrals over the line of propagation. To simplify the description of how $\bar{I}$ is evaluated numerically, we consider first the double integral, assuming that I is available at whatever angles and locations it is needed. For convenience here we write $I = I(\theta, t)$, but the reader should keep in mind that I depends on time only through $\mathbf{r}(t)$.

The first step is to replace the limits on the integral over θ with infinite limits:

$$\bar{I} = \frac{1}{t_M}\int_t^{t+t_M}\int_{-\infty}^{\infty} IG_w(\theta - \theta_a)d\theta dt'. \tag{6}$$

While strictly speaking this is an approximation, none has been indicated because the error it introduces is entirely negligible for the narrow beamwidths to be considered; $G_w(\theta - \theta_a)$ decreases so rapidly with θ that it is virtually zero outside the original limits. By changing variables from θ to x, (6) becomes

$$\bar{I} = \int_t^{t+t_M}\int_{-\infty}^{\infty} kI(\theta_a + \gamma x, t')e^{-x^2}dxdt', \tag{7}$$

where k and γ are constants. The double integral in (7) has the form needed to apply a formula for numerical integration which is a product of Gauss–Legendre and Gauss–Hermite quadrature formulas for integration over a single variable (the latter formula is convenient for handling the exponential weighting but its use requires the infinite interval). The theory of Gaussian quadrature and the construction of product formulas are discussed in Stroud (1971). With this formula the double integral is approximated by

$$\begin{aligned}\bar{I} &= \int\int kI(\theta_a + \gamma x, t')e^{-x^2}dxdt' \\ &\approx \sum_{i=1}^{n_H}\sum_{j=1}^{n_L} w_{ij}kI(\theta_a + \gamma x_i, t + t'_j),\end{aligned} \tag{8}$$

where n_H and n_L are the numbers of points in the Gauss–Hermite and Gauss–Legendre formulas, x_i and t'_j the abscissas, and w_{ij} the weights of the product formula. This is a *cubature* formula because it approximates a multiple integral. The use of (8) means that to compute $\bar{I}$ for one measurement it is necessary to evaluate I for lines of propagation at all combinations of n_H angles and n_L locations (because of aircraft movement the location of the antenna is different at each time). The choice of n_H and n_L is discussed below.

The radiance I is computed for lines of propagation required by (8) from the integral expressions that were

discussed above for the quantities appearing on the right-hand side of (1). The fields of atmospheric and cloud properties are represented with discretizations that permit these integrals to be evaluated analytically. The cloud is a rectangular array of n small square elements in each of which cloud properties such as α and temperature are constant, though they can vary from element to element. The cloud is embedded in a clear environment which consists of a rectangular array of 500 m squares with semi-infinite slabs of the same thickness on its flanks. As with the cloud, atmospheric properties are constant in each environmental element. The environment is 9 km deep, which is enough to include all the atmosphere with radiative properties significant for this study. Integrals such as those in (2) and (3) are evaluated as the sum of integrals over segments of the line of propagation which intersect cloud or environmental elements. The constancy of the atmospheric properties in the elements is what permits the latter integrals to be given by analytic expressions. In these expressions the lengths of the line segments as well as the values of atmospheric properties appear.

By substituting the formula for I in (8), we obtain the formula used to calculate the value of $\bar{I}$ for a measurement; the formulas for different measurements collectively give (except for the simulated measurement errors) a formula for $\tilde{\mathbf{I}}$. As will be discussed below, this formula is also used in the retrieval procedure, though many of the parameters used in it have different meanings and values.

b. A modified retrieval procedure

The problem of retrieval is to estimate the distribution of ρ_l that produced the radiative intensities in a set of measurements, simulated or real. The procedure followed in this study is similar to that described in WDK. The thermodynamic structure of the cloud's environment is specified from a sounding. An estimate is made of the distribution of α within the cloud. Associated with this estimate are certain implied average radiances that would be measured if the estimate of α were accurate. The implied average radiances, arranged in the same order as the measurements in $\tilde{\mathbf{I}}$, are considered together as a vector, $\mathbf{E}$. A new estimate of α in the cloud is made from the previous estimate and from $\mathbf{E} - \tilde{\mathbf{I}}$. This is repeated for a number of iterations. The retrieved distribution of ρ_l is inferred from what is left after gaseous absorption is subtracted from the final estimate of α. The principal difference between the old and new procedures is in how the new estimate of α is made.

The retrieval atmosphere and cloud are discretized in the manner just described for the simulation atmosphere and cloud. The α_j is defined to be the estimate of α in the jth cloud element, and $\boldsymbol{\alpha} = (\alpha_1, \alpha_2, \alpha_3, \cdots, \alpha_n)^T$. The finite antenna beamwidth and the effect of the antenna movement during a measurement are also represented for retrieval just as when generating synthetic measurements. So the same formula used to compute $\bar{I}$, except with estimates of the thermodynamic parameters of the atmosphere and cloud replacing those parameters specified in a simulation, is used to compute the implied average radiances which are the components of $\mathbf{E}$. It is convenient to represent this by the equation $\mathbf{E} = \mathbf{N}(\boldsymbol{\alpha})$, where N is the nonlinear function just defined.

The mathematical problem solved in retrieval is formulated as:

$$\min|\mathbf{E} - \tilde{\mathbf{I}}|$$

$$\text{such that } \alpha_j \geq \alpha g_j, \quad j = 1, 2, 3, \cdots, n. \tag{9}$$

The estimate of α is required to be no less than α_g because it is a physical constraint that should improve the accuracy of a retrieval (the reason for this is discussed in section 4b). Equation (9) is a problem in constrained, nonlinear programming which is solved in two steps. First, we solve

$$\min|\mathbf{E} - \tilde{\mathbf{I}}| \tag{10}$$

to obtain an unconstrained estimate of α, denoted by α^u. To do this requires knowledge of how $\mathbf{E}$ will vary with small changes in α. This information is given by $\mathbf{A}$, the $m \times n$ matrix of partial derivatives of components of $\mathbf{E}$ with respect to the α_j, that is, the Jacobian matrix of $\mathbf{E}$ with respect to α whose (i, j)th element is

$$a_{ij}(\boldsymbol{\alpha}) = \frac{\partial E_i}{\partial \alpha_j}; \tag{11}$$

a_{ij} is computed analytically from $\mathbf{N}(\boldsymbol{\alpha})$. In the second step we solve a local approximation to (9) which is derived as follows. Let $\mathbf{E}^u$ and $\mathbf{A}^u$ denote the values of $\mathbf{E}$ and $\mathbf{A}$ when $\boldsymbol{\alpha} = \boldsymbol{\alpha}^u$:

$$\mathbf{E}^u = \mathbf{N}(\boldsymbol{\alpha}_u)$$

$$\mathbf{A}^u = \frac{\partial \mathbf{N}}{\partial \boldsymbol{\alpha}}(\boldsymbol{\alpha}_u).$$

Here $\mathbf{N}(\boldsymbol{\alpha})$ may be expanded in a Taylor series about $\boldsymbol{\alpha} = \boldsymbol{\alpha}_u$ as

$$\mathbf{N}(\boldsymbol{\alpha}) = \mathbf{N}(\boldsymbol{\alpha}^u) + \mathbf{A}^u(\boldsymbol{\alpha} - \boldsymbol{\alpha}^u) + \mathrm{O}(|\boldsymbol{\alpha} - \boldsymbol{\alpha}_u|^2), \tag{12}$$

where $\mathrm{O}(x)$ stands for terms that, as x approaches zero, vanish at least as fast as x. The local approximation is obtained by substituting (12) in (9) and dropping terms higher than first order in $\boldsymbol{\alpha} - \boldsymbol{\alpha}^u$ to give:

$$\min|\mathbf{E}^u + \mathbf{A}^u(\boldsymbol{\alpha} - \boldsymbol{\alpha}^u) - \tilde{\mathbf{I}}|$$

$$\text{such that } \alpha_j \geq \alpha g_j. \tag{13}$$

The solution to (13) is denoted α^c, and the estimate of the liquid density in the jth element, $\hat{\rho} l_j$, is given by

$$\hat{\rho} l_j = \frac{(\alpha_j{}^c - \alpha g_j)}{\kappa_j} \geq 0, \tag{14}$$

where κ_j is the value of κ in the jth element. The solution to (10) is computed with the Levenberg–Marquardt algorithm for the nonlinear least-squares problem of Moré (1978) and the solution to (13) with the algorithm *wnnls* of Hanson and Haskell (1982).

c. *The choice of n_H and n_L*

Some preliminary simulation was necessary to determine acceptable values for n_H and n_L. It is desirable to keep them both as small as possible because the computational requirements are proportional to the number of cubature points. In these simulations the cloud was 4 km square, had a maximum liquid density of 2.5 g m^{-3}, and was divided into 64 elements; t_M was chosen to be 0.5 s.

For $n_L = 2$, samples of simulations were generated for beamwidths at 1° intervals between 1° and 6° with $n_H = 4$ and $n_H = 5$. From each sample of ten simulations the average rms error in ρ_l and its standard error were computed. The differences between the average rms errors for $n_H = 4$ and $n_H = 5$ were obviously within the standard errors for beamwidths less than 6°, but for 6° the average rms error was 0.257 ± 0.025 g m^{-3} when n_H was 4 and 0.125 ± 0.010 g m^{-3} when it was 5. Because of this difference it was deemed safer to use the larger value of n_H, though no results reported below are for beamwidths greater than 5°.

Simulations were performed with $n_H = 5$ for the six beamwidths to compare results for $n_L = 1$ and $n_L = 2$. The logarithms of the rms errors for a single simulation with each beamwidth for a given value of n_L were regarded as components of a random vector from a Gaussian distribution. The logarithmic transformation was made because the rms errors themselves are always positive, which would not be consistent with a Gaussian distribution. The samples for each value of n_L were compared by statistical hypothesis testing to determine if they were drawn from the same distribution.

First the hypothesis H_0, that the distribution had equal covariance matrices though possibly unequal means, was tested against the hypothesis H_1, that the matrices were unequal. Following the procedure described in Anderson (1984, p. 422), a statistic λ is computed which has a χ^2 distribution with 21 degrees of freedom. The critical region was taken to have a size of 0.05 and corresponded to $\lambda > 32.7$, meaning that if H_0 were true, a λ this large has only a 0.05 probability of occurring. If λ falls within the critical region, H_0 would be rejected in favor of H_1. Because λ was found to be 7.7, H_0 was accepted.

Then, under the assumption of equal covariance matrices, the hypothesis H_0, that the means of the distributions are equal, was tested against the hypothesis H_1 that they are unequal. Following the procedure of Anderson (1984, p. 338) a statistic λ is computed which has a χ^2 distribution with 6 degrees of freedom. The critical region with size 0.05 is $\lambda > 12.6$. The computed λ was 4.1, so H_0 was accepted. Therefore, since the rms errors for the two values of n_L seemed to be drawn from the same distribution, $n_L = 1$ was chosen for the retrieval algorithm. Thus each computed measurement is, effectively, an average over a beam, rather than over a beam blurred by movement of the antenna.

3. Results of simulation studies

The error in the retrieved ρ_l, denoted by ρ_l', for each combination of atmospheric, observational, and retrieval parameters is the mean of the rms errors from a sample of ten simulations. The aircraft carrying the radiometer flew 100 m below cloud base at a speed of 89 m s^{-1}. An aircraft traverse extended from where the cloud first was detected by the forward-pointing antenna to where it could last be detected by the aft-pointing antenna. Unless otherwise stated:

1) The aircraft flew with a nose-up attitude of 3.7° from the horizontal.

2) The radiometer antennas had 2° beamwidths and were elevated 45° from the longitudinal axis of the aircraft.

3) A radiometer measurement of brightness temperature had a standard deviation of 0.2 K for an integration time of 0.1 s. However, an averaging time t_M of 0.33 s was used.

4) The mean profiles of thermodynamic variables assumed for the cloud's environment, shown in Fig. 2, are representative of the autumn climate in coastal Louisiana.

These aircraft flight parameters, radiometer characteristics, and atmospheric profiles were chosen be-

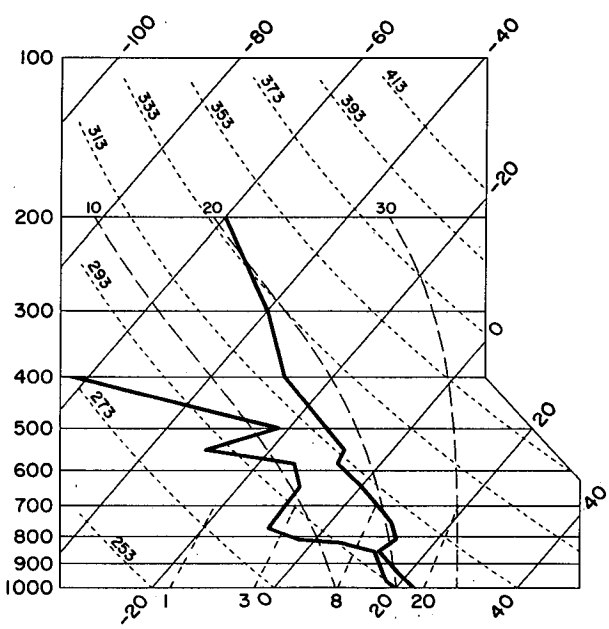

FIG. 2. Environmental sounding for an autumn day with nonprecipitating cumuli in southern Louisiana.

TABLE 1. Standard deviations of fluctuations of thermodynamic variables.

	Subcloud layer	Cloud environment				
		Altitude (km)				
	0–0.5	0.5–1.7	1.7–5.8	5.8–6.6	6.6–12	Cloud
σ_T (K)	1	0.5	0.5	0.5	0.5	0.5
σ_{ρ_v} (g m^{-3})	1	0.5	0.2	0.1	0.05	Dependent on temperature fluctuations through the saturation condition

cause they were typical of conditions during a field program described in Warner and Drake (1988). An averaging time of 0.33 s was used to prepare the field radiometric data from this program for retrieval.

To represent atmospheric variability when generating synthetic measurements, the temperature of an atmospheric element was drawn from a Gaussian distribution whose mean is equal to the mean temperature profile at the altitude of the element's center and whose standard deviation is given in Table 1. An analogous procedure was followed in assigning the humidity of environmental elements, while cloud elements were saturated. Knowledge of the horizontal variability of temperature and humidity was not assumed in retrieval from synthetic measurements, which used only the mean profiles. The simulated clouds had liquid water distributions that were asymmetrical with a central maximum; a typical example is given in Table 2.

The accuracy of a retrieval depends upon the number of measurements of given quality, the resolution demanded, and the liquid water content of the cloud. The size of a cloud element relative to the size of the cloud determines the number of elements. The ratio of the number of measurements to the number of elements, m/n, is a measure of how overdetermined the retrieval is; other things being equal, the more overdetermined the more accurate the retrieval. The time during a traverse in which useful measurements of a cloud of given size and shape can be made depends upon the aircraft speed and the vertical separation between the aircraft trajectory and cloud base. If these are considered fixed, then m is determined by the choice of averaging time. The emitted radiation from a cloud of given size increases with the amount of liquid (at least until the cloud is effectively a blackbody), reducing the relative importance of inaccurate measurements or (unknown) random fluctuations of temperature and humidity from their horizontal means. Hence the relative error in the retrieval, $\rho_l'/\rho_{l_{max}}$, should vary inversely with some function of $\rho_{l_{max}}$.

If ρ_l' is assumed proportional to a power of $\rho_{l_{max}}$, an exponent of 0.5 gives the best fit to the results from the retrievals reported here. This scaling is used in Fig. 3 to summarize the results for different resolutions, liquid amounts, and sizes and shapes of clouds as a function of m/n. The cloud elements were between 143 and 500 m in size. In addition to the results for the Louisiana climate, some results are presented of simulations with the thermodynamic profiles for summer in Colorado that were used in WDK. The scaled error clearly varies inversely with m/n and is less for the Colorado climate than for that of Louisiana. The figure also shows the relation between the element size or resolution and m/n for square clouds of given area. The resolution can be calculated from m/n and known parameters and is readily shown to vary only about 10% for ratios of cloud width to height between 0.25 and 4. To illustrate the use of Fig. 3, consider a square cloud in the Louisiana climate which is 2 km on a side with a maximum liquid density of 2 g m^{-3}. A retrieval with 400 m resolution requires (reading off the 4 km^2 line) about 11 times as many measurements as cloud elements (n = 25), which implies a value of $\rho_l'/\rho_{l_{max}}^{1/2}$ between 0.05 and 0.06, and thus an rms error of 0.07–0.08 g m^{-3}.

The lines labeled Louisiana and Colorado in Fig. 3 are least-squares fits to the results for the respective climates. The linear relation on a log–log plot implies

TABLE 2. Typical distribution of liquid density (g m^{-3}) used in simulations.

0.96	0.91	1.08	1.34	1.34	1.05	0.92	0.73	0.51	0.72	0.93	1.01
1.25	1.82	1.81	1.84	1.86	1.76	1.46	1.37	1.44	1.37	1.63	1.29
1.23	1.89	2.32	2.19	2.09	1.97	2.02	1.91	1.85	2.04	1.45	0.96
0.77	1.57	2.11	2.52	2.23	2.14	2.32	2.33	2.23	1.72	1.19	0.56
0.41	1.16	1.93	2.44	2.84	2.71	2.69	2.81	2.25	1.49	0.99	0.50
0.42	0.97	1.67	2.55	3.19	3.53	3.45	2.79	2.14	1.66	0.99	0.36
0.36	1.04	1.69	2.65	3.45	4.00	3.81	2.89	2.19	1.70	1.12	0.35
0.27	1.05	1.98	2.66	3.51	3.64	3.47	3.16	2.28	1.57	1.00	0.43
0.33	1.08	1.89	2.83	2.82	2.81	2.94	2.73	2.30	1.41	0.73	0.14
0.28	1.16	1.92	2.16	2.21	2.07	2.13	2.06	1.73	1.40	0.52	0.00
0.26	1.25	1.56	1.55	1.63	1.62	1.39	1.26	1.17	0.93	0.75	0.14
0.56	0.77	0.99	1.25	1.17	1.02	0.93	0.61	0.45	0.59	0.64	0.50

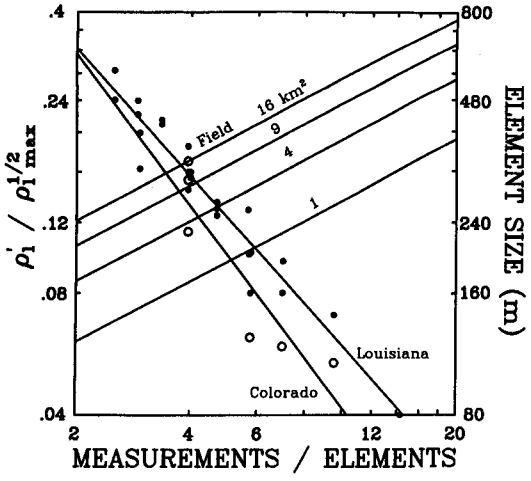

FIG. 3. The scaled error in retrieved liquid density from clouds of various sizes, resolutions, and shapes. Filled circles denote Louisiana climate, open circles the Colorado climate.

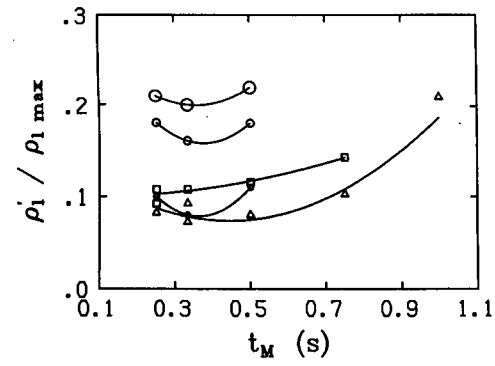

FIG. 4. Relative error as a function of the averaging time of each measurement. Large, medium, and small circles display results for a 1 km square cloud with $\rho_{l_{max}} = 1$ g m^{-3} divided into 49, 36, and 25 elements respectively. Squares and triangles display results for a 4 km square cloud with $\rho_{l_{max}} = 4$ g m^{-3} divided into 169 and 144 elements respectively.

that $(m/n)^{\mu}\rho_l'/\rho_{l_{max}}^{1/2}$ should be roughly constant for some μ. This fit to the scaled error has been used to present the data from which the figure was constructed in Table 3. The table does not reveal any obvious residual dependence upon the size, shape, or liquid water content of the cloud.

The curves in Fig. 4 show the variation in relative retrieval error with averaging time for retrievals of given resolution from clouds with given sizes and liquid amounts. The retrieval accuracy is not greatly affected by changes in the averaging time—at least between 0.25 and 0.75 s—because reducing the averaging time increases the number of measurements but also increases the measurement error. This result led us to choose an averaging time of 0.33 s.

TABLE 3. Fitted rms errors: $(m/n)^{\mu}\rho_l'/\rho_{l_{max}}^{1/2}$, where ρ_l' and $\rho_{l_{max}}$ are in g m^{-3} and the cloud size is the width and height in km.

		m/n										
$\rho_{l_{max}}$	Cloud size	2.5	2.9	3.4	3.9	4.0	4.7	5.7	5.8	7.0	9.6	14.3
						Louisiana, $\mu = 1.10$						
4.0	4 × 4	0.79	0.77	0.72	0.65		0.68			0.68		
					0.72		0.74					
	1.3 × 4											0.75
	1 × 4							0.68				
1.0	1 × 1		0.66			0.74			0.55			
	4 × 4	0.67	0.71	0.80	0.72		0.71		0.87	0.82		
0.5	4 × 1										0.85	
0.3	1 × 1		0.53			0.71			0.69			
						Colorado, $\mu = 1.31$						
2.5	4 × 4				0.69					0.75		
1.0	4 × 4				1.02							
0.6	1 × 1								0.61			
0.5	4 × 1										1.03	
0.3	4 × 4				0.92							

Changes in the sensitivity of the radiometer receiver directly affect the accuracy of retrieval. The receiver sensitivity is expressed as the standard deviation of measured brightness temperature for an integration time of 0.1 s. Thus Fig. 5 shows that for a fixed number of measurements, cloud size, resolution, and liquid water content, ρ_l' is roughly proportional to the receiver sensitivity. The finite value of ρ_l' for zero receiver noise is due to the unknown, random fluctuations in temperature and water vapor about their known mean profiles.

In Appendix A dimensional analysis is applied to the simulation results to derive a formula which relates ρ_l' to receiver sensitivity, aircraft speed, t_M, retrieval resolution, and the temperature, liquid content, and size of the cloud. A higher flight speed means less time to obtain measurements, and thus a smaller m and greater retrieval error. Raising the cloud temperature

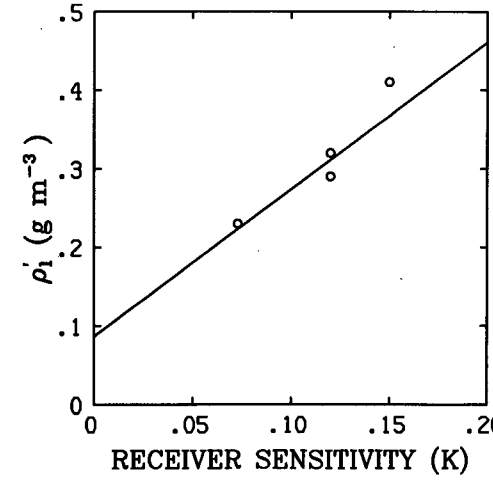

FIG. 5. The error in retrieved liquid density for different receiver sensitivities.

increases the Planck function, but (at least for the clouds simulated) reduces the emitted radiation because of a more rapid *decrease* of κ, the coefficient of liquid absorption and emission.

The errors in retrievals from simulated measurements made with antennas having 2° and 5° beamwidths are compared in Fig. 6. The simulated clouds were 1 and 4 km square and had maximum liquid water contents of 1 and 4 g m^{-3}, respectively. The $\rho_{l_{\max}}^{1/2}$ scaling is used because results for clouds with different liquid amounts are presented on the same figure. The retrieval error associated with the wider beam is, at most, slightly larger than with the 2° beam. This does not imply that the difference would remain small for still wider beams, or for bigger clouds or finer resolution than considered here, but does show that antennas with wider beams than those used in the field program referred to earlier could almost certainly be used in future work. The advantage in this is that such antennas are smaller. At the frequency in use, a 5° beam is obtainable from an antenna 15 cm in diameter which would have much less drag than those actually used and could possibly be mounted on a smaller aircraft.

The effect of small changes of the antenna elevation angle on retrieval accuracy was considered in two simulations in which the antennas were elevated 40° and 50°. The 4 km square cloud that was simulated had a $\rho_{l_{\max}}$ of 4 g m^{-3} and was divided into 144 elements. For elevations of 40° and 50° the respective values of ρ_l' were 0.52 and 0.50 g m^{-3}. The comparable values for the numbers of simulated measurements (626 and 520) from the fit in Fig. 3 are 0.28 and 0.36 g m^{-3}. If changing the elevation angle has no effect, the errors for the different angles should be close to the fitted line, but the differences are somewhat larger than what scatter would usually produce. A more likely reason for these differences is discussed in the following section.

4. A local analysis of the radiative transfer equation

The error in a retrieval of ρ_l is associated with the indeterminacy of the result of inverting a set of measurements: the data are roughly consistent with a number of different distributions of cloud liquid. The ambiguity arises from two sources. The radiometric measurements and the environmental quantities obviously have uncertainties which make any estimate of ρ_l somewhat indefinite. But even were they known precisely, a distribution of cloud liquid compatible with the measurements is not unique. A complete analysis of the possible ambiguities would be difficult if not impossible, even for a single dataset, because the radiative transfer equation is nonlinear, but we believe the local analysis of this equation which follows reveals some of the more important, qualitative consequences of ambiguity.

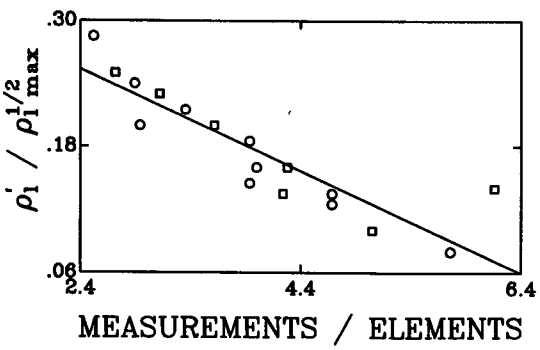

FIG. 6. A comparison of the scaled errors associated with beamwidths of (circle) 2° and (square) 5° vs the ratio of measurements to elements.

In the first part of the analysis the discrete, radiative transfer equation is linearized to consider the spatial distribution of error when the true and retrieved cloud liquid distributions are both represented by the cloud elements discussed in section 2. In the second part, the *original* radiative transfer equation is linearized to consider how a wider class of liquid distributions is mapped into the space of radiances to be measured. The analysis of the discrete equation elucidates principally the uncertainty in the retrieval due to uncertainty in the measured quantities, while pointing towards the question of inherent nonuniqueness, which the analysis of the "continuous" equation addresses.

a. Discrete analysis

Depending on how a retrieval is used the spatial distribution of the error might be as important as its overall magnitude. The true field of cloud water, the pattern of measurements, and the choice of how the cloud is discretized imply a certain set of characteristic error modes. These modes and measures of their corresponding likelihoods may be found by performing a singular value analysis on a local approximation to the governing radiative transfer operator.

In this subsection we neglect the difference between the error modes of the total absorption coefficient and those of the liquid water density and, except as noted later, the effect of inequality constraints on retrieved quantities. In the clouds of interest α_g is generally much less than α, and the spatial variation of κ, while quantitatively important, will not affect the qualitative conclusions that we shall draw.

A local, linear approximation to (9) which is analogous to (13) may be written as

$$\mathbf{A}^*(\alpha - \alpha^*) + \mathbf{E}^* \approx \tilde{\mathbf{I}}, \tag{15}$$

where α^* is the true vector of cloud absorption coefficients, $\mathbf{A}^*$ and $\mathbf{E}^*$ are the values of $\mathbf{A}$ and $\mathbf{E}$ when $\alpha = \alpha^*$, and all other quantities assume their true values. If $\mathbf{e}_\alpha = \alpha - \alpha^*$ and $\mathbf{e}_I = \tilde{\mathbf{I}} - \mathbf{E}^*$ are the respective errors in the vectors of absorption coefficients and measured intensities, then (15) implies that

$$\mathbf{A}^*\mathbf{e}_\alpha \approx \mathbf{e}_I. \tag{16}$$

TABLE 4. Columns of V associated with σ.

				σ_{63}			
0.00	0.00	−0.01	0.03	−0.04	0.01	0.00	0.00
0.00	0.03	−0.08	0.12	−0.13	0.09	−0.03	0.00
−0.01	0.08	−0.16	0.28	−0.26	0.18	−0.08	0.01
−0.03	0.10	−0.25	0.32	−0.35	0.22	−0.10	0.03
−0.02	0.10	−0.19	0.31	−0.27	0.20	−0.08	0.02
−0.01	0.05	−0.13	0.17	−0.19	0.10	−0.04	0.01
0.00	0.02	−0.05	0.08	−0.06	0.05	−0.01	0.00
0.00	0.00	−0.01	0.02	−0.02	0.00	0.00	0.00
				σ_{64}			
0.00	0.00	0.00	0.00	0.01	0.01	0.00	0.00
0.00	0.00	0.04	0.07	0.06	0.03	0.00	0.00
0.00	−0.07	−0.16	−0.19	−0.21	−0.13	−0.07	−0.01
0.03	0.11	0.22	0.36	0.31	0.24	0.10	0.03
−0.03	−0.10	−0.25	−0.30	−0.33	−0.23	−0.11	−0.03
0.01	0.07	0.13	0.22	0.21	0.15	0.07	0.02
0.00	−0.02	−0.06	−0.08	−0.09	−0.07	−0.03	0.00
0.00	0.00	0.01	0.02	0.03	0.02	0.00	0.00

The singular value decomposition allows $\mathbf{A}^*$ to be expressed as

$$\mathbf{A}^* = \mathbf{U}\begin{bmatrix}\mathbf{S}\\ \mathbf{0}\end{bmatrix}\mathbf{V}^T = [\mathbf{U}_1\mathbf{U}_2]\begin{bmatrix}\mathbf{S}\\ \mathbf{0}\end{bmatrix}\mathbf{V}^T, \qquad (17)$$

where $\mathbf{U}$ and $\mathbf{V}$ are orthogonal matrices with dimensions $m \times m$ and $n \times n$ respectively, $\mathbf{U}_1$ and $\mathbf{U}_2$ are $m \times n$ and $m \times (m - n)$ submatrices, and $\mathbf{S} = \text{diag}(\sigma_1, \cdots, \sigma_n)$, with $\sigma_1 \geq \sigma_2 \geq \cdots \geq \sigma_n > 0$; the σ_j are the singular values of $\mathbf{A}^*$ (cf. theorem 4.1, Lawson and Hanson 1974; it is assumed here that $\mathbf{A}^*$ has full rank). The least-squares solution of (16) then takes the form

$$\mathbf{e}_\alpha = \mathbf{V}\mathbf{S}^{-1}(\mathbf{U}_1^T\mathbf{e}_I) = \mathbf{V}\mathbf{S}^{-1}\mathbf{b}. \qquad (18)$$

It is evident from (18) that $\mathbf{e}_\alpha$ is a linear combination of columns of $\mathbf{V}$, weighted by the reciprocals of the corresponding singular values. Suppose $\mathbf{e}_I$ is drawn from a multivariate normal distribution with zero mean and a diagonal covariance matrix with all the variances equal to σ_I^2. The same is then true of $\mathbf{b}$ since the rows of $\mathbf{U}_1^T$ (columns of $\mathbf{U}_1$) are orthonormal. But while any direction of $\mathbf{b}$ is thus equally likely, $\mathbf{e}_\alpha$ has preferred directions because the singular values are, in general, unequal. Hence, the most likely pattern of error is a distribution associated with a multiple of the last column of $\mathbf{V}$, the next most likely that associated with the next to last column, and so forth. The columns of $\mathbf{V}$ are proportional to the principal components of the covariance matrix of $\mathbf{e}_\alpha$ (see theorems 2.4.1 and 11.2.1 in Anderson 1984).

The two most dominant error modes, i.e., columns of $\mathbf{V}$, for a 4 km square cloud consisting of 64 elements with a maximum liquid density of 4 g m^{-3}, observed from an aircraft that flies with an attitude of 3° carrying radiometers elevated 45° are presented in Table 4. The top of an array corresponds to the top of the cloud. The most obvious features of these modes are the alternating rows and columns with elements of opposite signs. These features are typical of the corresponding error modes for all the different patterns of airborne radiometer measurements that have been analyzed and are the consequence of the tomographic analysis of data with an extremely limited angular distribution, i.e., only two angles. This is discussed more in the next subsection. Most of the measurements are affected by elements from several rows or columns. Since the contribution of each element is additive (at least in the local approximation) relatively large amplitudes of the dominant error modes can thus be present in a retrieval because partial cancellation reduces their effect on the length of the residual vector, $\mathbf{A}^*\mathbf{e}_\alpha - \mathbf{e}_I$.

A pattern of measurements or a liquid distribution making cancellation more complete should then also increase the error; one such pattern might be that from an aircraft flying with an attitude of 0°. The antennas will here point in directions parallel to the diagonals of the array of elements, making this pattern an extreme of symmetry for the assumed discretization, and the associated average error is likely either to be very large or very small. By simulating this pattern the error was found to be 0.96 g m^{-3} in comparison to the value of 0.12 g m^{-3} expected from the fit shown in Fig. 3. This large difference suggests that cancellation is important and may be more so when the antennas point in directions nearly parallel to the diagonals of elements. This would explain the surprising sensitivity to the elevation angle of the antennas noted at the end of the previous section: with an attitude of 3.7° and antennas elevated 40° the forward pointing antenna is 43.7° from the horizontal while with antennas elevated 50° the rearward pointing antenna is 46.3° from the horizontal. In each case the beams from one antenna were nearly parallel to the diagonals.

If the proximity of the antenna directions to the diagonals tends to increase the error then the size of the smallest singular value should be roughly proportional to the average absolute deviation of antenna direction from the nearest diagonal. This may be seen in Fig. 7, where the smallest singular values for several different choices of antenna elevation and aircraft attitude are plotted against the average absolute deviation for all measurements. The singular values are normalized by m to correct for the direct effect of changes in the number of measurements.

The consistent pattern of the dominant error modes shown in Table 4 suggests that the retrieval accuracy might be improved by making measurements in additional directions. Even just one more antenna, pointing vertically, would virtually suppress the error mode with columns of alternating signs.

Taking into account the effect of the inequality constraints requires only a slight modification of the explanation given above. In the unconstrained, least-squares problem there is no strict limit to the amplitude of an error mode, making the average accuracy of a retrieval extremely dependent on the size of the smallest singular value. The requirement that the liquid density be nowhere negative limits the combined effect of all error modes. While the dominant error modes will remain so, their amplitudes are subject to the overall bound.

b. *Analysis of the "continuous" equation*

In this subsection we consider the information about α in the cloud, and thus ρ_l, that can be obtained without representing it as a function having only a finite number of free parameters. It is assumed that:

1) the antenna beams are infinitesimal and will be referred to as rays,

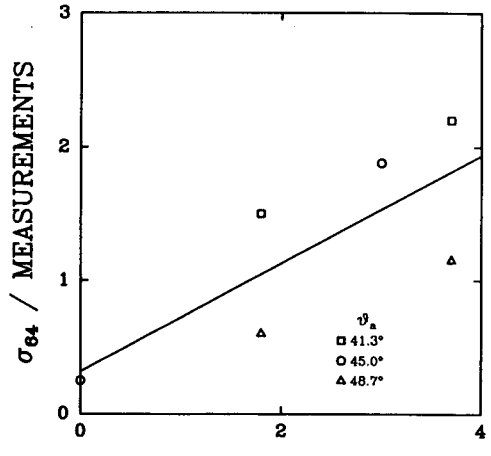

FIG. 7. The smallest singular value scaled by the number of measurements vs the average absolute deviation in angle from the direction of the element diagonals.

2) the environmental parameters are perfectly known,

3) the radiances are measured continuously and without error,

4) an estimate of the absorption coefficient in the cloud, α_0, is available that is close enough to the true one that all nonlinear functions can be accurately replaced with linear approximations.

The goal of the retrieval problem that will be posed is to find $\alpha' = \alpha - \alpha_0$. It is shown below that, in general, this is impossible. What can be found is the closest approximation to α' having the form $k_1 f + k_2 g$, where k_1 and k_2 are specific functions and f and g have certain symmetries but are otherwise arbitrary. For instance, if the aircraft attitude is constant during a traverse so the directions of the antennas do not vary,

$$\nabla f \cdot \mathbf{a}_1 = \nabla g \cdot \mathbf{a}_2 = 0,$$

where $\mathbf{a}_i$ is a unit vector with the same direction as the ith antenna. Therefore, the part of α' that can be determined lies in a fairly restricted class of functions. Following the proof of these assertions is a discussion of their significance.

The region containing the cloud is denoted by Γ. Since I_l and τ_l are known from the environmental parameters it is convenient to define a shifted, scaled radiance, $R \equiv (I - I_l)/\tau_l$. Substituting this definition and (3) in (1) and rearranging terms then gives

$$R = \int_{s_1}^{s_2} B\alpha\tau(s_1, s')ds' + \tau_c I_u. \tag{19}$$

Linearizing (19) about α_0 gives

$$R' = \int_{s_1}^{s_2} \alpha' K ds', \tag{20}$$

where $R' = R - R_0$, $R_0 = R(\alpha_0)$, and K is a function which depends on the location of the antenna and the path length along the ray.

Let each measurement be associated with the horizontal coordinate of the antenna at the time of measurement. The data consist of two sets of measurements, one from each antenna. Suppose that every point in Γ has one and only one ray from each set passing through it (this will be so if excursions of aircraft attitude are not too large). Then there is a one-to-one mapping from Γ into the set of pairs of rays from the two antennas. Let each pair be labeled by (s, t), where s and t are the associated antenna coordinates, and let the mapping from a point $\mathbf{r}$ in physical space to a point ρ in "antenna" space be given by $\rho(\mathbf{r}) = (s, t)$ (cf. Fig. 8). The image of Γ under this mapping will be denoted by Γ'. Dropping the primes from the perturbation radiance R', (20) may be written separately for each antenna as

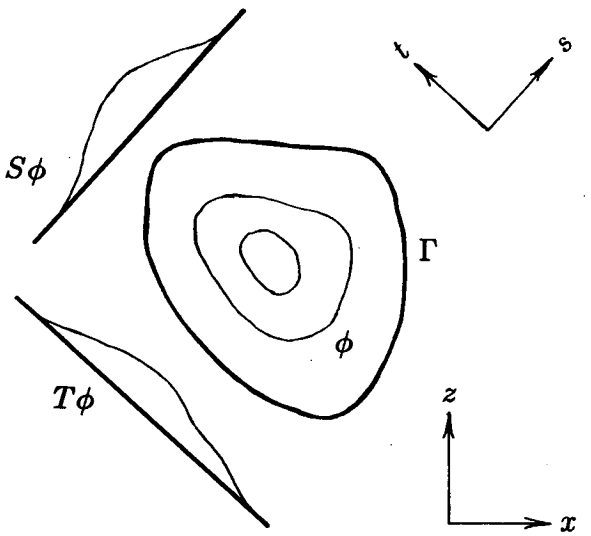

FIG. 8. A distribution ϕ defined in the region Γ, with its projections $S\phi$ and $T\phi$ onto the s and t axes.

$$R_1(s) = \int \alpha'(r_1)K_1(s, s')ds',$$

$$R_2(t) = \int \alpha'(r_2)K_2(t, s')ds', \qquad (21)$$

where $r_1 = r_1(s, s')$ and $r_2 = r_2(t, s')$ parameterize the rays through the cloud from the two antennas and R_1, R_2 and K_1, K_2 are the functions R and K for the respective antennas. Let $\phi[\rho(r)] = \phi(s, t) = \alpha'(r)$; α' and ϕ are assumed to be absolutely integrable on Γ and Γ', respectively. Defining

$$k_1(s, t) \equiv K_1[s, l_1(t)] \frac{dl_1}{dt}$$

$$k_2(s, t) \equiv K_2[t, l_2(s)] \frac{dl_2}{ds},$$

where l_i is the path length along the ray from the ith antenna, (21) may be written

$$R_1(s) = \int \phi k_1 dt \equiv S\phi,$$

$$R_2(t) = \int \phi k_2 ds \equiv T\phi, \qquad (22)$$

where the equations define the linear integral operators S and T.

Let P be the subspace of functions defined on Γ' such that if $p \in P$ then $p = k_1 p_1(s) + k_2 p_2(t)$, where p_1 and p_2 are absolutely integrable. Then ϕ may be written as $\phi = \phi_P + \phi_\perp$, where $\phi_P \in P$ and $\phi_\perp \in P^\perp$, $P^\perp$ being the orthogonal complement of P (Taylor and Lay 1980, p. 89). The ϕ_P and $\phi_\perp$ are the projections of ϕ onto P and $P^\perp$, respectively. It is shown in appendix B that R_1 and R_2 determine ϕ_P uniquely. It may then be expressed as $k_1 f(s) + k_2 g(t)$. However, $S\phi_\perp = T\phi_\perp = 0$, which makes it impossible to determine $\phi_\perp$ from R_1 and R_2 because a different distribution of liquid associated with $\tilde{\phi} = \phi_P + \tilde{\phi}_\perp$, $\tilde{\phi}_\perp \neq \phi_\perp$, has the same perturbation radiances and is thus indistinguishable from ϕ_P. So P is the space of determinate or retrievable distributions and $P_\perp$ the space of irretrievable or indeterminate distributions. The importance of the indeterminancy of the projection of ϕ onto $P_\perp$ should not, however, be overrated.

First, the indeterminacy arises in the context of a linearization that is valid only when α' is small. This restriction extends to the indeterminate part of α'—it cannot be so large as to render the linear approximation invalid. Second, the scientific significance of the possibility that spatial distributions of liquid may be only partly determinate can neither be assessed a priori nor with the observations of clouds made before the Louisiana field program mentioned above. For instance, however accurate a sequence of in situ measurements of ρ_l from an aircraft making a single pass through a cloud, nothing from it can be deduced about the partition of spatial variance between determinate and indeterminate parts of α'. Finally, the present analysis suggests that the *projection* of the liquid distribution onto the space of determinate distributions, P, can be inferred quite accurately if α can be estimated closely enough for a linear approximation to be valid (cf. the example in appendix B).

The character of the retrievable part of the liquid distribution was discovered only after the simulations were done. Even so, the liquid distributions that were specified may have been inadvertently easy or difficult to retrieve by being more or less "parallel" to P. To consider this possibility, a rough estimate was made of the retrievable spatial variation in the distribution of liquid water content shown in Table 2. The ρ_l was taken to be proportional to α, and it was assumed that k_1 and k_2 could be approximated by constants. The aircraft attitude was varied between $-5°$ and $5°$. Under these assumptions the distribution was decomposed into projections onto P and $P^\perp$ using Fourier analysis. The retrievable component was found to account for 63% of the second moment of the distribution, so the simulations do not appear to have been unduly biased either towards or against accurate retrievals.

When a retrieved projection is intended to approximate the liquid distribution it makes sense to use the inequality constraint on α, e.g., when comparing a retrieved estimate of ρ_l to an in situ measurement representative of a small part of a vertical cross section. In other situations an accurate estimate of the projection itself (which of course can physically assume negative values) might be more of interest. A proposition concerning the statistics of the distribution of liquid in clouds, whether deduced from theory or simply intended as a descriptive summary, implies another proposition about the statistics of projections of the

distribution whose truth can be tested against estimates made by cloud tomography.

5. The effect of large drops

For ρ_l to be retrieved unambiguously it must be proportional to the liquid absorption coefficient; this relation holds strictly only when all drops are small in comparison to the wavelength. To better understand the limitation this requirement imposes on cloud tomography, Mie theory was used to compute the absorption and scattering by drop spectra having concentrations of large drops within the range of interest. Each spectrum consisted of some small droplets together with a distribution of drops from either the Marshall–Palmer or Sekhorn–Srivastava families or Blanchard's observations of nonorographic rain in Hawaii (Pruppacher and Klett 1980). The nominal mass density of small droplets was taken to be 0.5 g m^{-3}, an autoconversion threshold which is frequently used with the parameterization of Kessler (1969). Results for all three drop size distributions were closely similar.

Figure 9 shows how the effective absorption coefficient per unit mass density of liquid water varies with the precipitation rate; evidently it does not change by more than 25% for rates below several mm h^{-1}. The amount of scattering relative to absorption is also shown to increase with the amount of precipitation. A scattering coefficient that is 10% of the maximum absorption coefficient would not be negligible for a retrieval and thus limits the acceptable amount of precipitation to be no greater than roughly 1 mm h^{-1}. The precise upper limit necessarily depends on the actual drop distribution in a cloud as well as the intended application of the technique.

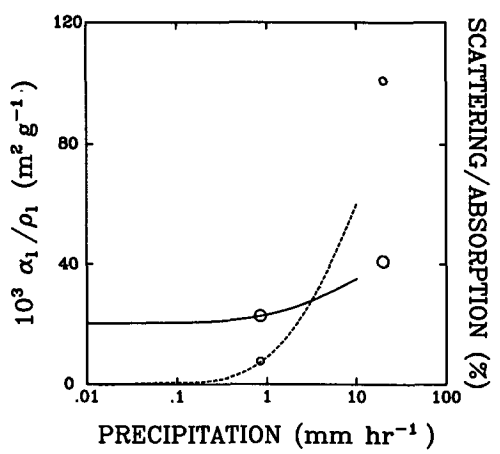

FIG. 9. The ratio between the absorption coefficient (m^{-1}) computed from Mie theory and liquid density (g m^{-3}) and the ratio between scattering and absorption coefficients as functions of precipitation rate assuming 0.5 g m^{-3} of infinitesimal droplets to be added to the raindrop spectra. The first ratio is plotted with a solid curve for the Marshall–Palmer and the Sekhorn–Srivastava families and large circles for Blanchard nonorographic rain, and the second ratio with a dashed curve and small circles, respectively.

6. Conclusions

Certain general limitations on the use of tomography previously noted for a ground-based system using two coplanar scanning antennas remain applicable to the airborne configuration discussed here. The data for a single retrieval must be obtained in a time short enough that changes in the liquid distribution are negligible. Clouds suitable for study are either nonprecipitating or only slightly precipitating and may not contain melting ice particles. A cloud must be separate enough from its nearest neighbors for their emissions not to affect the measurements. Within these limits, however, the results of simulation studies of the airborne configuration show it to be as capable as the ground-based in accurately determining cross sections of the liquid water field.

The beamwidth of the antennas was found to be not critical, at least over the range of 2° to 5° for clouds of moderate size. The characteristic patterns of retrieval error found by singular value analysis suggest that an additional antenna would improve retrieval accuracy. In the present paper the analysis was performed knowing a priori the linearized, radiative transfer operator, but there is nothing to prevent a similar analysis being done with, e.g., the Jacobian matrix deduced from a set of real measurements, which would permit the assessment of how likely it is that a feature of interest in the retrieved field is an artifact of measurement error.

Acknowledgments. The authors wish to thank Dr. Kunio Shimizu of the Science University of Tokyo, for his advice in developing statistical procedures to decide what resolution was needed in the numerical cubature, and Dr. William A. Cooper, for drawing our attention to the question of the uniqueness of retrieval. We also gratefully acknowledge the assistance of B. Brock Wakham and Christian Host in programming and performing simulations.

APPENDIX A

Dimensional Analysis of the Retrieval Error

The dependence of the estimated retrieval error, ρ_l', on a number of parameters under standard conditions (e.g., fixed aircraft speed and measurement time) was presented in Fig. 3. It also seems to be possible to describe its variation more generally with a formula derived by combining dimensional analysis of the simulation results with certain principles that either are directly supported by the results or are plausible theoretically.

It is conjectured that the most important, physical quantities determining ρ_l' are:

T_o the rms error in the measured brightness temperature when the measurement is averaged for an integration time t_o

t_M the averaging time
v the aircraft speed
θ a characteristic cloud temperature taken to be the (absolute) temperature at the center of the cloud
K a characteristic value of κ, taken to be $\kappa(\theta)$
R a characteristic cloud liquid density, taken to be $\rho_{l_{\max}}$
l the geometric mean of the lengths of sides of the cloud rectangle
b the size of an element in the retrieval.

Equation (12) implies that

$$\rho_l' \approx \frac{T_o}{\kappa\sigma_n}\left(\frac{t_o}{t_M}\right)^{1/2} \tag{A1}$$

where σ_n is the smallest singular value. The following nondimensional quantities are

$$\begin{aligned} \sigma^* &\equiv KR\sigma_n/\theta, \\ \rho^* &\equiv \rho_l'/R, \\ T^* &\equiv T_o/\theta, \\ t^* &\equiv t_M vKR, \\ t_o^* &\equiv t_o vKR, \\ l^* &\equiv lKR, \\ b^* &\equiv b/l. \end{aligned} \tag{A2}$$

Equation (A1) may then be written nondimensionally as

$$\rho^* = \frac{T^*}{\sigma_*(b^*, l^*, t^*)}\left(\frac{t_o^*}{t^*}\right)^{1/2}. \tag{A3}$$

The first principle is that ρ_l' is insensitive to changes in t_M, implying

$$\rho^* = T^*\sqrt{t_o^*}\,g(b^*, l^*) \tag{A4}$$

where g is a dimensionless function. The next principle is that for fixed R, T^*, t_o and cloud size, ρ_l' is simply a function of m/n, or equivalently of $b^{*2}l^*$, i.e.,

$$\rho^* = T^*\sqrt{t_o^*}\,h(b^{*2}l^*). \tag{A5}$$

The (unscaled) results of the simulations that are scaled and presented in Table 3, when made dimensionless with (A2), imply that $\ln h \approx 3.70 - 0.923 \ln b^{*2}\, l^*$ (with correlation coefficient > 0.99), from which it follows that

$$\rho_l' \approx 40.4\,\frac{T_o}{\theta}\sqrt{vt_oK}\left(\frac{l}{b^2K}\right)^{0.923}\rho_{l_{\max}}^{0.577}. \tag{A6}$$

APPENDIX B

Analysis of Retrievable Distributions and an Example

We may assume without loss of generality that $\Gamma' \subset (0, 1) \times (0, 1)$. The theorems and pages referred to below are in Taylor and Lay (1980). Let X, Y and Z be the real Hilbert spaces $L^1(\Gamma')$, $L^1(0, 1)$ and $Y \times Y$, respectively, and let B be the linear operator mapping $x \in X$ into the pair $(Sx, Tx) \in Z$, where S and T are defined in (22). When $y \in Z$ we write

$$y = [y_1(s), y_2(t)].$$

The inner product on X is defined as

$$(x, u) = \int\int_{\Gamma'} xu\,ds\,dt, \quad x, u \in X,$$

and on Z as

$$(y, z) = \int y_1 z_1\,ds + \int y_2 z_2\,dt, \quad y, z \in Z.$$

Because B is densely defined in X it has an adjoint, B^*, which maps Z into X. For every y in the domain of B^* there is a unique element, $\omega = B^*y$, of X such that for every x in X, $(Bx, y) = (x, \omega)$ (p. 242).

$$\begin{aligned} (Bx, y) &= \int\left(\int xk_1\,dt\right)y_1\,ds + \int\left(\int xk_2\,ds\right)y_2\,dt \\ &= \int\int_{\Gamma'} xk_1y_1\,ds\,dt + \int\int_{\Gamma'} xk_2y_2\,ds\,dt \\ &= \int\int_{\Gamma'} x(k_1y_1 + k_2y_2)\,ds\,dt = (x, \omega), \end{aligned}$$

where the replacement of the iterated integrals by the double integrals is justified by Fubini's theorem (e.g., p. 229). Since ω is unique, $B^*y = k_1y_1(s) + k_2y_2(t)$.

Every ϕ in X may be represented uniquely in the form $\phi = r + \phi_\perp$, where $\phi_\perp \in N(B)$, the null space of B, and $r \in N(B)^\perp$, its orthogonal complement (theorem II.7.4). B is a continuous operator on X, so it is closed (theorem IV.5.1). This implies that $N(B)^\perp = \overline{R(B^*)}$ (p. 244), where $R(B^*)$ denotes the range of the operator B^* and the overbar denotes the closure of a set. Since X, the domain of B, is closed and B is closed, $R(B)$ is closed (p. 209). Then $R(B^*)$ is also closed (theorem IV.11.2), so $R(B^*) = \overline{R(B^*)} = N(B)^\perp$ and $r \in R(B^*)$. In the preceding paragraph it was shown that this implies $r = k_1f(s) + k_2g(t)$, so $\phi = k_1f(s) + k_2g(t) + \phi_\perp$, where $f, g \in Y$. If C is the restriction of B to the domain $N(B)^\perp$ then C has an inverse (theorem I.3.1) which evidently maps $[f, g]$ into r.

An especially illuminating example is that of $\Gamma = (0, 1) \times (0, 1)$, and $k_1 = k_2 = 1$. Suppose $S\phi = f(s)$

and $T\phi = g(t)$. For consistency, it is necessary that $Tf = Sg$, which is constant. It is easy to see that $r = f + g - Sg$, for

$$Sr = Sf + Sg - S^2g = f + Sg - Sg = f,$$

$$Tr = Tf + Tg - TSg = g + Tf - Tf = g.$$

In this instance r differs only by a constant from the sum of the projections of ϕ onto the s and t axes.

REFERENCES

Anderson, T. W., 1984: *An Introduction to Multivariate Statistical Analysis.* 2nd ed., Wiley & Sons, 675 pp.

Hanson, R. J., and K. Haskell, 1982: Two algorithms for the linearly constrained least-squares problem. *ACM Trans. Math. Soft.*, **8**, 323–333.

Kessler, E., 1969: On the distribution and continuity of water substance in atmospheric circulation. *Meteor. Monogr.*, **10**, No. 32.

Lawson, C. L., and R. J. Hanson, 1974: *Solving Least-Squares Problems.* Prentice-Hall, 340 pp.

Moré, J. J., 1978: The Levenberg–Marquardt algorithm: Implementation and theory. *Numerical Analysis,* G. A. Watson, Ed., Springer-Verlag, 105–116.

Pruppacher, H. R., and J. D. Klett, 1980: *Microphysics of Clouds and Precipitation.* Reidel, 714 pp.

Stroud, A. H., 1971: *Approximate Calculation of Multiple Integrals.* Prentice-Hall, 431 pp.

Taylor, A. E., and D. C. Lay, 1980: *Introduction to Functional Analysis.* 2nd ed., Wiley & Sons, 467 pp.

Warner, J., and J. F. Drake, 1988: Field tests of an airborne remote sensing technique for measuring the distribution of liquid water in convective cloud. *J. Atmos. Oceanic Technol.*, **5**, 833–843.

——, —— and P. R. Krehbiel, 1985: Determination of cloud liquid water distribution by inversion of radiometric data. *J. Atmos. Oceanic Technol.*, **2**, 293–303.

——, —— and J. Snider, 1986: Liquid water distribution obtained from coplanar scanning radiometers. *J. Atmos. Oceanic Technol.*, **3**, 542–546.